Highly functionalized organic nitrates in the southeast United States: Contribution to secondary organic aerosol and reactive nitrogen budgets

Ben H. Lee[a,1], Claudia Mohr[a,1,2], Felipe D. Lopez-Hilfiker[a], Anna Lutz[b], Mattias Hallquist[b], Lance Lee[c,3], Paul Romer[c], Ronald C. Cohen[c], Siddharth Iyer[d], Theo Kurtén[d], Weiwei Hu[e,f], Douglas A. Day[e,f], Pedro Campuzano-Jost[e,f], Jose L. Jimenez[e,f], Lu Xu[g], Nga Lee Ng[g,h], Hongyu Guo[h], Rodney J. Weber[h], Robert J. Wild[f,i], Steven S. Brown[i], Abigail Koss[i], Joost de Gouw[f,i], Kevin Olson[j,4], Allen H. Goldstein[j], Roger Seco[k], Saewung Kim[k], Kevin McAvey[l], Paul B. Shepson[l], Tim Starn[m], Karsten Baumann[n], Eric S. Edgerton[n], Jiumeng Liu[o], John E. Shilling[o], David O. Miller[p], William Brune[p], Siegfried Schobesberger[a], Emma L. D'Ambro[q], and Joel A. Thornton[a,5]

[a]Department of Atmospheric Sciences, University of Washington, Seattle, WA 98195; [b]Department of Chemistry and Molecular Biology, Atmospheric Science, University of Gothenburg, SE-41296 Gothenburg, Sweden; [c]Department of Chemistry, University of California, Berkeley, CA 94720; [d]Department of Chemistry, Laboratory of Physical Chemistry, University of Helsinki, Helsinki FIN-00014, Finland; [e]Department of Chemistry and Biochemistry, University of Colorado Boulder, Boulder, CO 80309; [f]Cooperative Institute for Research in Environmental Sciences, University of Colorado Boulder, Boulder, CO 80309; [g]School of Chemical and Biomolecular Engineering, Georgia Institute of Technology, Atlanta, GA 30332; [h]School of Earth and Atmospheric Sciences, Georgia Institute of Technology, Atlanta, GA 30332; [i]Chemical Sciences Division, National Oceanic and Atmospheric Administration, Boulder, CO 80305; [j]Department of Environmental Science, Policy and Management, University of California, Berkeley, CA 94720; [k]Department of Earth System Science, School of Physical Sciences, University of California, Irvine, CA 92697; [l]Departments of Chemistry and Earth, Atmospheric and Planetary Sciences and Purdue Climate Change Research Center, Purdue University, West Lafayette, IN 47907; [m]Department of Chemistry, West Chester University, West Chester, PA 19383; [n]Atmospheric Research and Analysis, Inc., Cary, NC 27513; [o]Atmospheric Sciences and Global Change Division, Pacific Northwest National Laboratory, Richland, WA 99352; [p]Department of Meteorology, Pennsylvania State University, University Park, PA 16802; and [q]Department of Chemistry, University of Washington, Seattle, WA 98195

Edited by John H. Seinfeld, California Institute of Technology, Pasadena, CA, and approved December 16, 2015 (received for review April 24, 2015)

Speciated particle-phase organic nitrates (pONs) were quantified using online chemical ionization MS during June and July of 2013 in rural Alabama as part of the Southern Oxidant and Aerosol Study. A large fraction of pONs is highly functionalized, possessing between six and eight oxygen atoms within each carbon number group, and is not the common first generation alkyl nitrates previously reported. Using calibrations for isoprene hydroxynitrates and the measured molecular compositions, we estimate that pONs account for 3% and 8% of total submicrometer organic aerosol mass, on average, during the day and night, respectively. Each of the isoprene- and monoterpenes-derived groups exhibited a strong diel trend consistent with the emission patterns of likely biogenic hydrocarbon precursors. An observationally constrained diel box model can replicate the observed pON assuming that pONs (*i*) are produced in the gas phase and rapidly establish gas–particle equilibrium and (*ii*) have a short particle-phase lifetime (~2–4 h). Such dynamic behavior has significant implications for the production and phase partitioning of pONs, organic aerosol mass, and reactive nitrogen speciation in a forested environment.

particulate organic nitrates | online measurement | lifetime calculation | high-resolution time-of-flight chemical ionization mass spectrometer | biogenic volatile organic compound oxidation

Organic nitrates (ONs; ON = $RONO_2$ + RO_2NO_2) are an important reservoir, if not sink, of atmospheric nitrogen oxides (NO_x = NO + NO_2). ONs formed from isoprene oxidation alone are responsible for the export of 8–30% of anthropogenic NO_x out of the US continental boundary layer (1, 2). Regional NO_x budgets and tropospheric ozone (O_3) production are, therefore, particularly sensitive to uncertainties in the yields and fates of ON (3–6). The yields implemented in modeling studies are determined from laboratory experiments, in which only a few of the first generation gaseous ONs or the total gas-phase ONs and particle-phase organic nitrates (pONs) have been quantified, whereas production of highly functionalized ONs capable of strongly partitioning to the particle phase have been inferred (7–11) or directly measured in the gas phase (12). Addition of a nitrate (–ONO_2) functional group to a hydrocarbon is estimated to lower the equilibrium saturation vapor pressure by 2.5–3 orders of magnitude (13). Thus, ON formation can enhance particle-phase partitioning of semivolatile species in regions with elevated levels of nitrogen oxides, contributing to secondary organic aerosol (SOA) growth (8). However, highly time-resolved measurements of speciated ON in the particle phase have been lacking.

We use a recently developed high-resolution time-of-flight chemical ionization mass spectrometer (HRToF-CIMS) using iodide-adduct ionization (14) with a filter inlet for gases and aerosols (FIGAERO) (15) that allows alternating in situ measurements of the molecular

Significance

We present online field observations of the speciated molecular composition of organic nitrates in ambient atmospheric particles utilizing recently developed high-resolution MS-based instrumentation. We find that never-before-identified low-volatility organic species, which are highly functionalized, explain a major fraction of the total particle nitrate mass measured by the traditional aerosol mass spectrometer. An observationally constrained box model shows that these organic nitrates are likely derived from oxidation of biogenic hydrocarbons and persist in the particle phase for only a few hours. Given their high rate of loss, their fates have significant implications for the budgets of secondary organic aerosol particles and nitrogen oxides but are currently unknown.

Author contributions: J.A.T. designed research; C.M., F.D.L.-H., A.L., M.H., P.R., R.C.C., S.I., T.K., W.H., D.A.D., P.C.-J., J.L.J., L.X., N.L.N., H.G., R. J. Weber, R. J. Wild, S.S.B., A.K., J.d.G., K.O., A.H.G., R.S., S.K., K.M., P.B.S., T.S., K.B., E.S.E., J.L., J.E.S., D.O.M., W.B., S.S., and E.L.D. performed research; L.L., J.L., and J.E.S. contributed new reagents/analytic tools; B.H.L. analyzed data; and B.H.L. wrote the paper.

The authors declare no conflict of interest.

This article is a PNAS Direct Submission.

[1]B.H.L. and C.M. contributed equally to this work.

[2]Present address: Institute of Meteorology and Climate Research, Atmospheric Aerosol Research, Karlsruhe Institute of Technology, 76344 Eggenstein-Leopoldshafen, Germany.

[3]Present address: Chemical Sciences Division, Lawrence Berkeley National Laboratory, Berkeley, CA 94720.

[4]Present address: Chevron Products Company, Richmond, CA 94802.

[5]To whom correspondence should be addressed. Email: thornton@atmos.washington.edu.

This article contains supporting information online at www.pnas.org/lookup/suppl/doi:10.1073/pnas.1508108113/-/DCSupplemental.

www.pnas.org/cgi/doi/10.1073/pnas.1508108113

composition of gas and particle phases. We present observations of speciated ON in the particle phase obtained during the 2013 Southern Oxidant and Aerosol Study (SOAS) in the southeast United States. We analyze the diel cycles of individual components using a 0D box model to elucidate differential source and sink terms. Biogenic volatile organic compounds (BVOCs), including isoprene and monoterpenes, seem to dominate the ON sources during the SOAS. We show that the molecular compositions that dominate the particle phase are significantly more oxygenated than the most abundant gas-phase counterparts, consistent with volatility and solubility-driven partitioning requirements. Although the detailed chemical mechanisms by which these atmospheric ONs form are not explicitly derived here, we observed compounds possessing the same molecular compositions with similar relative distributions in controlled chamber experiments simulating BVOC oxidation under both daytime and nighttime conditions (shown in *SI Appendix*, Figs. S1 and S2). Such speciated ON measurements in both the field and the laboratory (*i*) put a strong constraint on the extent to which ONs directly contribute to SOA in regions with high-biogenic hydrocarbon emissions, (*ii*) illustrate that the fate of particulate ONs can have significant implications for SOA and the reactive nitrogen budget, and (*iii*) provide guidance for the types of ON formation mechanisms needing elucidation.

Methods

The FIGAERO HRToF-CIMS instrument was housed in an air-conditioned trailer located in a clearing near Centreville, Alabama (33.18 °N, 86.78 °W) during June and July of 2013 as part of the SOAS. Site description and instruments involved during the SOAS campaign are detailed elsewhere (8, 16–18). Ambient air was continuously drawn with mechanical pumps through two inlets. One inlet was a 2.7-m long, 2.5-cm o.d. (~2.2-cm i.d.) stainless steel tube fitted with a custom inertial impactor to remove particles >~2 μm through which ~22 standard L/min (slpm) was drawn through a 1-μm-pore size perfluorotetrafluoroethylene filter in the FIGAERO unit to collect particles [Reynold's number (R_e) ~ 1,850]. The second inlet was 1.8-m long, 1.9-cm o.d. (~1.6-cm i.d.) perfluorotetrafluoroethylene tubing through which ~16 slpm was drawn for gas-phase measurements (R_e ~ 1,350). Particles were collected for 20 min during gas-phase measurements and then immediately subjected to a temperature-programmed thermal desorption in 2.5 slpm ultrahigh-purity (UHP) N_2. The UHP N_2 during the desorption was gradually heated at 10 °C/min from ambient temperature to 200 °C and then, held at 200 °C for 25 min, which was sufficiently long for signals to return to background levels, ensuring complete desorption. A second particle filter was programmatically placed upstream of the normal particle filter on every fourth desorption. This approach provided a way to correct for any interfering background signal that may arise from semi- and nonvolatile gases that can collect on filters as well as artifacts originating from the ionization source (19).

The HRToF-CIMS allows for the determination of molecular ion composition but not molecular structure. Thus, aside from some basic rules, we cannot distinguish between peroxy nitrates and multifunctional alkyl nitrates. We rule out oxygenated amines as contributing to our signals, which are dominated by C_5 and C_{10} compounds, because there is no evidence of C_5 and C_{10} amine precursors. We include in our analysis only nitrogen-containing organic compounds with chemical formulas consistent with an ON (one N atom, an odd number of H atoms, and three or more O atoms or in the case of a dinitrate, two N atoms, an even number of H atoms, and at least six O atoms) that are attached to an iodide ion and have mass concentrations >0.1 ng m^{-3} over the 20-min collection period.

The HRToF-CIMS was calibrated for three isomers of isoprene hydroxynitrate ($C_5H_9NO_4$) (20). The iodide-adduct ionization is most sensitive to polar organics with hydroxy groups (14), and the dominant ON signal in the particle phase observed during the SOAS was of highly oxygenated compounds. As such, we apply the highest sensitivity value obtained (8.5 counts $second^{-1}$ per parts per trillion per million total reagent ion) from these calibrations—that of the β-4,3 isomer of $C_5H_9NO_4$, with structure that presumably allows the iodide ion to interact most stably with the hydroxy functional group—to all observed ONs to calculate the mass concentration (micrograms $meter^{-3}$) of each. The two other isomers (*cis* and *trans* δ-1,4) of isoprene hydroxynitrate were detected less sensitively by this technique likely because of the location of the hydroxy functional group relative to that of the nitrate, which can increase the polarity of the hydroxy group and therefore, the stability of the iodide–hydroxynitrate adduct (*SI Appendix*). Sensitivity generally increases with increasing functionality and increasing number of atoms on the molecule but not indefinitely (14). Our reported mass concentrations would be higher by a factor of ~2.2 if we applied the mean sensitivity of the *cis* and *trans* δ-1,4 and lower by a factor of ~2.5 if we applied the highest sensitivity to any compound tested thus far using iodide-adduct HRToF-CIMS.

Simple alkyl or keto nitrates are underestimated or not detected at all. Indeed, the technique is nearly an order of magnitude less sensitive to peroxy acetyl nitrate than to the isoprene hydroxy nitrates, and thus, any peroxy acyl nitrate (five or more O atoms) would be greatly underestimated unless it had at least one or more hydroxy groups in addition to the nitrate moiety. Such multifunctional peroxy acyl nitrates have not been reported, although their presence in the atmosphere cannot be ruled out. Our focus herein is on pONs measured after thermal desorption. Thus, it is unlikely that peroxy nitrates are a large fraction of the detected pON, even if they are present in the particle, because of their propensity to thermally dissociate into nitrogen dioxide (NO_2), which we do not detect, and an organic fragment. The bulk of detected pON compounds desorbed between 60°C and 100 °C, where thermal loss of a nitrate moiety from alkyl nitrates should be negligible but where thermal decomposition of peroxy nitrates could be substantial (21). Aside from the peroxy nitrates, we expect thermal decomposition of most other organic functional groups at these temperatures to be minor (15), but perturbation of oligomer-like compounds in dynamic equilibrium with monomers is still a possibility. Unexpectedly large signals from particle desorption during the SOAS campaign often led to elevated backgrounds in the gas-phase detection mode, which in some cases, precluded quantitative comparisons between our gas-phase ON and pON measurements.

Multiple instruments probed the chemical composition of submicrometer atmospheric particles during the SOAS. Particle-phase alkyl nitrates were measured as gaseous NO_2 after thermal dissociation of pONs using the thermal dissociation laser-induced fluorescence instrument (TD-LIF) (22, 23). Total pONs (sum of alkyl, aromatic, peroxy, and peroxyacyl nitrates) were measured using two high-resolution time-of-flight aerosol mass spectrometers (HRToF-AMSs) using different ON calculation techniques. The University of Colorado Boulder group used the measured ratios of NO_2^+ to NO^+ ions in the mass spectra to distinguish ON from inorganic nitrate (7, 24), whereas the Georgia Institute of Technology group calculated ON as the difference between the HRToF-AMS–measured total nitrate and inorganic nitrate measured by the particles-into-liquid sampler ion chromatography instrument (25). The HRToF-AMS and TD-LIF methods are expected to quantitatively measure the total of all ON molecules in the particle phase. Sulfated organonitrates (26), presumably detected as particle nitrates by both the HRToF-AMS and TD-LIF techniques, were likely not strong contributors during the SOAS.

Results and Discussion

We identified 88 molecular compositions (*SI Appendix*, Fig. S3 and Table S1) consistent with an ON during the SOAS campaign. Fig. 1*A* shows a subset of the time series of total pONs as measured by two HRToF-AMSs, the FIGAERO HRToF-CIMS, and the TD-LIF when there was adequate data overlap between all techniques. A diurnal pattern with higher mass loadings at night compared with day was typically observed by all instruments (Fig. 1*B*) listed in *SI Appendix*, Table S2. We observed good correlation between the nitrate mass equivalent (NO_3^-; *m/z* 61.988 Th) of the sum of speciated pON measured by the FIGAERO HRToF-CIMS and that of total pON reported by the two HRToF-AMSs (*SI Appendix*, Table S2). The slight underestimation by the FIGAERO HRToF-CIMS relative to the HRToF-AMS technique may be because of the lower sensitivity to certain nitrates and/or thermal decomposition of undetected products. Nevertheless, these findings suggest that a significant fraction (at least 58%) of the pON budget as defined by the HRToF-AMS techniques is explained by the sum of the speciated pON as measured by the FIGAERO HRToF-CIMS to within the calibration uncertainty of the iodide-adduct ionization technique.

In general, the various measures of pON were well-correlated. The TD-LIF measurements exhibited reasonable correlation to the mass spectrometric methods but were, on average, higher by a factor of ~5 compared with those of the FIGAERO HRToF-CIMS (*SI Appendix*, Table S2). Measurements by the TD-LIF and the HRToF-AMS provide a reasonable range of pONs present during the SOAS, whereas the FIGAERO HRToF-CIMS provides molecular identification of individual species that

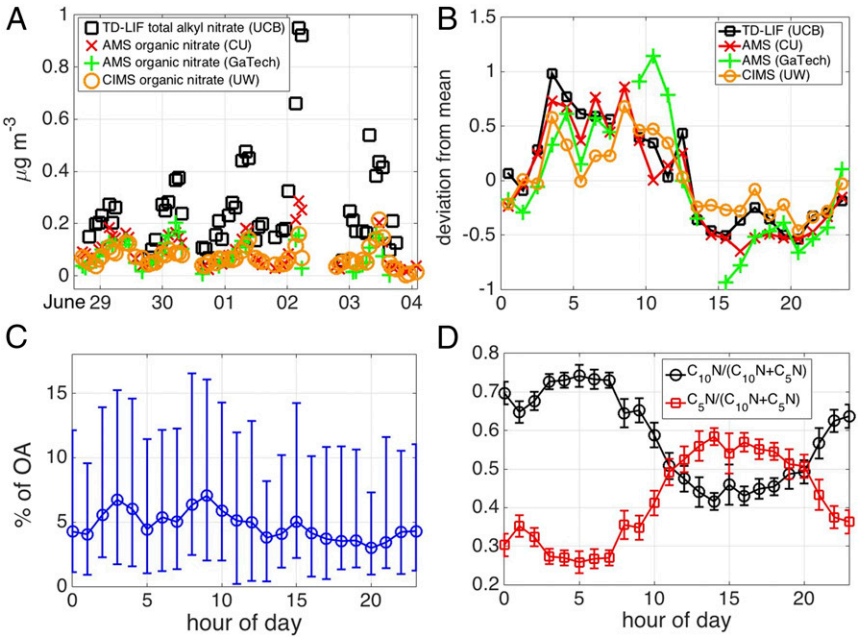

Fig. 1. (*A*) Subset of the time series of total pON as measured by two HRToF-AMSs, the FIGAERO HRToF-CIMS, and the TD-LIF during the SOAS. (*B*) Deviation of each technique from their respective campaign means plotted as a function of time of day. Because of the sparse data overlap between the four techniques, we include data for all periods when there is overlap with the UW data. (*C*) Median contribution of the pON—accounting for their identified molecular masses—to measured OA plotted as a function of day. The lower and upper error bars represent 25th and 75th percentiles, respectively, of the observed atmospheric variability (systematic errors are discussed in the text). (*D*) Fractions of the C_5 (red) and C_{10} (black) ON groups contributions relative to their sums plotted as a function of time of day. CU, University of Colorado Boulder; GaTech, Georgia Institute of Technology; UCB, University of California, Berkeley; UW, University of Washington.

make up pONs. Although the reason for the discrepancy in absolute pON values between the multiple techniques is still under investigation, the main conclusions presented here are not strongly affected by this discrepancy. We focus on the lifetime of ON in the particle phase given the diurnal variability of pON, which is similarly observed by all of the techniques (Fig. 1*B*). We stress that the impacts of pON on SOA and reactive nitrogen budgets that we derive here, based on our FIGAERO HRToF-CIMS estimates (and those of the HRToF-AMS), will be even larger and thus, more important if the amount of pON is higher as reported by the TD-LIF. We also show that similar pON lifetimes are inferred, regardless of which dataset is used (*SI Appendix*).

Converting the sum of all 88 pON compounds measured by the FIGAERO HRToF-CIMS into an organic aerosol (OA) mass concentration using the molecular composition information, we find that pON contributed, on average, 3% and 8% at day (1200–1600 h local time) and night (2200–0500 h), respectively, to the total submicrometer OA mass as measured by the HRToF-AMS (Fig. 1*C*). This contribution is comparable with that reported recently for the Centreville, Alabama site, where unspeciated pONs were 6–10% of OA (27). To investigate further the nature of this diurnal cycle in the pON contribution to OA, we separated the pON species into those having 5 or 10 carbon atoms. In Fig. 1*D*, we show the contributions of the C_5 and C_{10} pON groups relative to the sum of the two as a function of time of day. The C_{10} pONs accounted for more mass during nighttime than during daytime, whereas the C_5 pONs exhibited the opposite trend, consistent with the typical levels of their assigned gaseous parent compounds—monoterpenes and isoprene (and/or 2-methyl-3-buten-2-ol), respectively (*SI Appendix*, Fig. S4).

The facts that the simple carbon number-based classes exhibit such clear and distinct diel trends relative to one another and that they are also consistent with the corresponding diel cycles of the biogenic hydrocarbon precursors strongly suggest that pON abundance is governed by processes occurring on a timescale of a few hours. Gas-phase production with dynamic gas–particle partitioning followed by rapid loss, such as by photolysis (28, 29), heterogeneous hydrolysis (30–33), or reaction with the hydroxyl radical (OH) (34, 35), could potentially operate on such timescales and have different patterns as a function of time of day between the C_5 and C_{10} groups. We note that the volatile organic compound + NO_3 and RO_2 + NO reactions produce varying levels of primary/secondary vs. tertiary ONs, all of which having different hydrolysis rates (30, 32, 33). Thus, the overall contribution of the various loss pathways to pON lifetime warrants additional studies.

We also note that the dominant molecular compositions of the pON are not consistent with commonly reported first generation ON produced from these BVOCs. Each pON possessed at least 4 and as many as 11 oxygen atoms. Within a group of pON having the same carbon number, a bell-shaped distribution was exhibited in the mole fraction of the total pON as a function of oxygen atom content. The highest contribution typically came from ON having between six and eight O atoms as illustrated in Fig. 2*A*, where the SOAS mean contribution of C_5 and C_{10} ON groups is plotted as a function of the detected *m*/*z*. Such a distribution is consistent with the combined effects of gas-phase abundance, which exhibits a decreasing trend with increasing oxygen atom number (Fig. 2*B*), and volatility/solubility trends with increasing functional groups. That is, compounds with fewer O atoms but similar numbers of C and H atoms may be more abundant in the gas phase but are less likely to partition to the condensed phase. As noted above, the chemical compositions of the observed pON have generally not been reported in previous laboratory studies. The first evidence for such ON in the gas phase was reported by Ehn et al. (12, 36) from studies of α-pinene oxidation. We find the same highly oxygenated ON (*SI Appendix*, Figs. S1 and S2) in chamber studies of both monoterpenes and isoprene oxidation in the presence of nitrogen oxides. Recent work with a similar methodology also shows highly oxygenated ON from other monoterpenes (37). Moreover, the fact that the relative abundances of species within each carbon number group differ between the particle (Fig. 2*A*) and gas (Fig. 2*B*) phases strongly suggests that the observed distributions are not the sole result of instrument sensitivity.

Therefore, it is reasonable to expect that most of the pON observed during the SOAS arises from first or second generation gas-phase byproducts of biogenic hydrocarbons with oxidation that is initiated by the nitrate radical (NO_3) or by O_3 or OH in the presence of NO_x. For example, $C_{10}H_{17}NO_7$ contributed the most to pON mass during the early morning hours (Fig. 3) immediately after sunrise (~0530 h local time) when the level of NO is highest because of NO_2 photolysis in the surface layer (38, 39). The gas-phase abundances of a number of C_{10} ONs also exhibit sharp increases during this period when the level of monoterpenes is

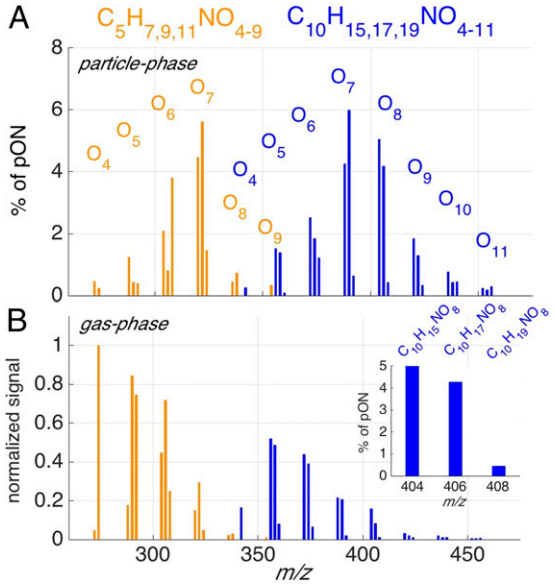

Fig. 2. Mole fractions of C_5 (gold) and C_{10} (blue) to total pON as defined by the FIGAERO HRToF-CIMS as a function of *m/z* (includes mass of I^- ion; *m/z* 126.905 Th). (*A*) Each carbon number group in the particle phase exhibits a bell-shaped distribution, with the dominant contribution from ON typically comprising between six and eight oxygen atoms. (*B*) Signal strength of the same ON in *A* but in the gas phase and normalized by the signal of $C_5H_9NO_4$. *B*, *Inset* is the same spectrum as in *A* at *m/z* 404, 406, and 408 Th, showing that, for each oxygen number, there are three ONs consisting of 15, 17, and 19 H atoms, respectively. C_5 ON species tend to possess 7, 9, or 11 H atoms. The gas phase shows a decreasing trend with increasing oxygen number. The exceptions are the low signals associated with $C_5H_7NO_4$ (*m/z* 271.943 Th) and $C_{10}H_{15}NO_4$ (*m/z* 340.005 Th), likely aldehyde or keto nitrates, which are not sensitively detected by iodide-adduct ionization (14).

rapidly decreasing (*SI Appendix*, Fig. S5). Reaction between a functionalized monoterpene-derived RO_2 radical (such as $C_{10}H_{17}O_6\bullet$) and NO could provide an explanation of such a diel pattern.

To test the likely sources and loss rates of the above pON groups, we constructed a box model constrained extensively by observations. For simplicity, we assumed that all C_5 pONs are derived from isoprene oxidation and that all C_{10} pONs are derived from oxidation of monoterpenes. The pONs are produced at a rate proportional to isoprene-RO_2 or monoterpene-RO_2 reacting with NO and isoprene and monoterpenes reacting with NO_3. The proportionality constant is, therefore, an effective yield of pON formation that incorporates the branching ratios for gas-phase ON formation across the distribution of multigeneration oxidation products correlated with the BVOC precursors as well as Raoult's or Henry's law-driven gas–particle partitioning coefficients. A suite of model runs was conducted, varying the effective yields of the RO_2 + NO (α_1) and NO_3 (α_2) reaction pathways, their temperature dependence, and the diurnally constant loss coefficient for each pON group. The presumed precursor BVOC and oxidant concentrations are constrained to their SOAS mean diurnal profiles (*SI Appendix*, Fig. S4). The differential equations governing production and loss are solved for multiple model days with diurnally repeating constraints until the diurnal profiles of the mass concentrations of C_5 and C_{10} pONs each establish steady state. The influence of boundary-layer height changes is implicitly accounted for by using diel profiles of observed mixing ratios of gaseous precursors and oxidants. Comparing the diel profiles of C_5 and C_{10} pONs with those of black carbon and the sulfate content in aerosol particles, both of which are comparatively longer lived, show that these trends are not driven by boundary-layer dynamics (*SI Appendix*, Fig. S6). However, because we cannot easily account for boundary layer dynamics because of unknown vertical profiles, we optimize the model–observation comparison excluding these transition periods and instead, focus on periods when the measurements represent a reasonably consistent layer height (2200–0500 and 1200–1600 h local time). Additional details of the box model are included in *SI Appendix*.

Observed (black in Fig. 4 *A* and *B*) and modeled (red in Fig. 4 *A* and *B*) C_5 and C_{10} pON mass concentrations are shown in Fig. 4 *A* and *B* plotted as a function of time of day. As the effective mole yields increase, so must the loss rates for the observation–model slope to be near one (*SI Appendix*, Fig. S7 *A* and *B*). A narrow range of pON loss rates exists, outside of which the observation–model correlation degrades (*SI Appendix*, Fig. S7 *C* and *D*). A similar relationship is observed between pON loss rates and temperature dependence of the effective yields (*SI Appendix*, Fig. S8). Varying the effective mole yields or its temperature dependence alone or together but not the pON loss rates cannot reproduce the observations. Although we applied a temperature dependence, such that the effective yields are higher at night than at day, with a diurnally constant loss rate, a faster loss rate during the day than at night with diurnally constant effective yields can give the same results. Applying effective yields for the NO_3 and RO_2 + NO reaction pathways as illustrated in Fig. 4 *C* and *D*, with loss rates for both C_{10} and C_5 pONs of $(1.0 \pm 0.3) \times 10^{-4}$ s^{-1} (2.1- to 4.0-h lifetime), resulted in optimal model–observation agreement with respect to slope and correlation (C_{10}: $R^2 = 0.85$ and slope = 0.86; C_5: $R^2 = 0.63$ and slope = 0.96). The fact that the effective yields for C_{10} pON are greater than those determined for C_5 pON is consistent with higher mass compounds being less volatile and alkyl nitrate branching ratios being greater for larger compounds (40, 41). Moreover, the effective yield for the monoterpene + NO_3 pathway is greater than that of monoterpene-RO_2 + NO, which is also expected given the high molar ON yields for most monoterpenes + NO_3 pathways found in the literature (42). The isoprene + NO_3 effective yield only weakly influences the modeled C_5 pON mass concentration, because the level of NO_3 radical is low when that of isoprene is high and as such, could not be robustly optimized. The good agreement between predictions

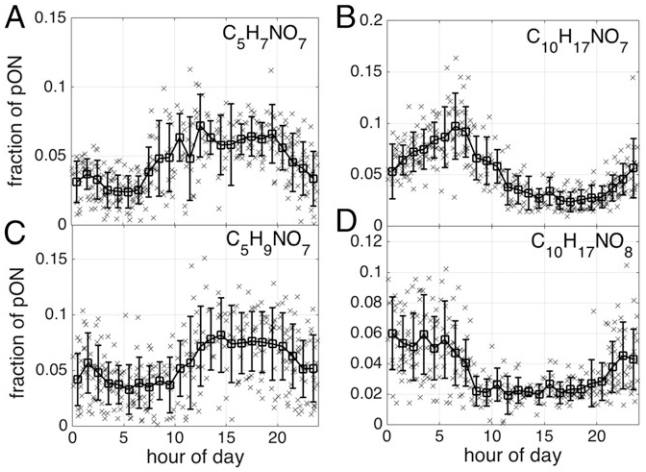

Fig. 3. Hourly (x) and campaign average (□) fraction of select pONs to the total pONs plotted as a function of time of day. Species in a given carbon number subgroup can exhibit similar but not identical diel trends. For instance, whereas the abundance of (*A*) $C_5H_7NO_7$ is immediately enhanced following sunrise (~0530 h), that of (*C*) $C_5H_9NO_7$ starts to increase around 1100 h (local). Diel trends for (*B*) $C_{10}H_{17}NO_7$ and (*D*) $C_{10}H_{17}NO_8$ are also similar, but not identical.

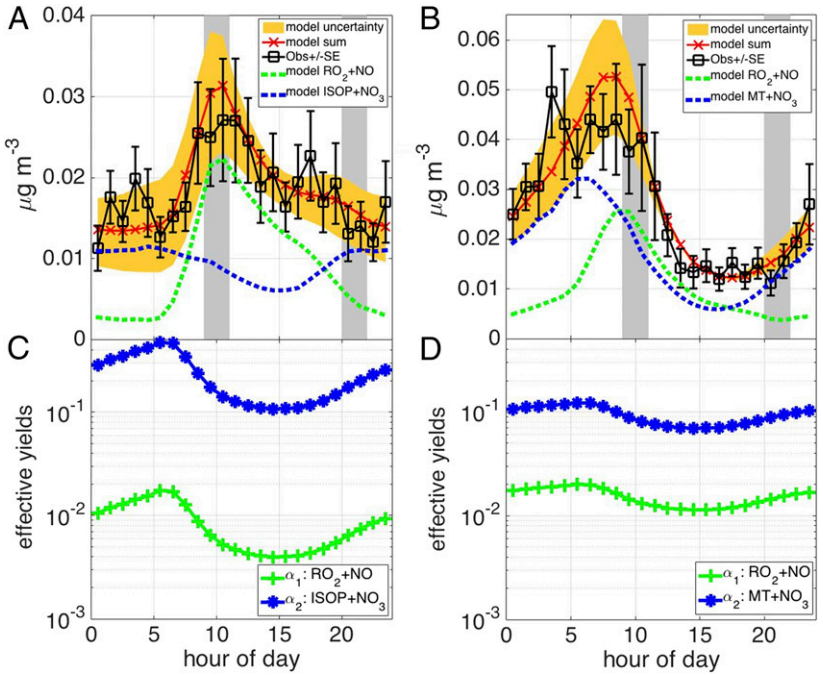

Fig. 4. Mass concentrations of observed (black) and modeled (red; *A*) C_5 and (*B*) C_{10} pON plotted as a function of time of day. Effective yields for the (α_1) RO_2 + NO and (α_2) NO_3 reaction pathways that yielded the best model observation agreement given loss rates for (*C*) C_5 and (*D*) C_{10} pON of $(1.0 \pm 0.3) \times 10^{-4}$ s^{-1} (2.1- to 4.0-h lifetime). Error bars on the observations represent the SE ($\sigma/\sqrt{n}$) of the SOAS mean. The gray shaded regions show the periods when the boundary layer height was changing rapidly (*SI Appendix*, Fig. S14), and they were consequently excluded for model optimization. ISOP, isoprene; MT, monoterpenes.

from a simple observationally constrained box model and measured pON mass concentrations provides support for the basic mechanistic components: (*i*) there is rapid pON formation from gas-phase oxidation of BVOCs with temperature-dependent effective yields, and (*ii*) the rate of pON loss is faster than the typical loss rate of atmospheric submicrometer particles because of dry and wet deposition (43). A similar pON lifetime (3.6 h) is obtained by comparing the instantaneous production rate—using 125 hourly averaged data points when there was overlap between all necessary measurements—with the observed sum pON (*SI Appendix*, Fig. S9).

There are several potentially important implications for regional atmospheric chemistry that would arise from pON having lifetimes of the order of a few hours. First, although the pON to OA ratio measured during the SOAS was typically low, at around 3–8% (Fig. 1*B*), it remains to be determined how much of the measured OA was the result of pON chemistry. If pON loss occurs by cleavage of the nitrate functional group from the carbon chain, while the bulk of the carbon mass remains in the particle phase, then the flux of ON through the particle phase could represent a substantial SOA source. For example, assuming molecular weights equivalent to $C_5H_{10}O_4$ and $C_{10}H_{18}O_4$ after the loss of an $-ONO_2$ group from the most abundant ON, we calculate that a total (not net) of 14.3 μg m^{-3} d^{-1} C_5 and C_{10} ON passes through the particle phase. Second, pON loss could represent a sink of atmospheric NO_x if the nitrate group is converted, presumably by hydrolysis, to nitric acid (HNO_3) (4, 33, 44, 45). Alternatively, if the nitroxy group is converted to nitrous acid (HONO) (46), the formation and subsequent loss of pON would be an NO_x null cycle but a source of HO_x after HONO photolysis. The production of HNO_3 (or HONO) because of total pON loss at a rate of 1×10^{-4} s^{-1} would be ~0.2 ppb d^{-1} compared with 0.5 ppb d^{-1} HNO_3 production rate from the reaction of NO_2 with OH.

Although this simple modeling framework explains the average behavior of groups of speciated ON, determining the governing chemical pathways for each pON remains a challenge. Even pONs of the same carbon atom number (for example, $C_{10}H_{17}NO_7$ and $C_{10}H_{17}NO_8$) exhibit similar but not identical diel trends (Fig. 3). The fraction of $C_{10}H_{17}NO_7$ to total pON continues to increase from sunset to sunrise, whereas that of $C_{10}H_{17}NO_8$ remains relatively flat after its initial evening increase, pointing to different chemical mechanism (RO_2 + NO derived vs. NO_3 derived), differing rates of gas-phase oxidation by OH and NO_3, varying particle-phase lifetimes that depend on molecular structure (32, 44, 47), and/or different BVOC precursors (e.g., α-pinene vs. limonene, isoprene nitrate dimers, etc.). The C_5 pONs are generally greater during the daytime than the nighttime, and likewise, species within this carbon atom number group can exhibit slightly different diel trends, as shown in Fig. 3 for $C_5H_7NO_7$ and $C_5H_9NO_7$ (both observed products of isoprene oxidation) (*SI Appendix*, Fig. S2).

As noted at the outset, our sum of speciated pON mass concentrations is on the lower end of other pON measurements made at the same location using different techniques. We selected a subset of detected ON species for analysis using a set of conservative criteria for identifying ON compositions that could be easily linked to isoprene and monoterpenes oxidation products. If we included all compounds in our spectra assigned to be ON, including dinitrates, then our total pON values would be about a factor of 1.5 greater. We potentially underestimate pON for that reason alone. Therefore, the above direct contributions of pON to SOA budget and NO_x cycling are likely underestimated. For example, we apply the model described above to the pON values reported by the TD-LIF. Good agreement between model and observation requires the same loss rate in the particle phase but with greater pON yields (*SI Appendix*, Fig. S10). The same loss rate and higher average abundance would imply a much higher contribution to SOA and impact on the NO_x budget than we discuss above.

Conclusions

We present observations of speciated pONs made on an hourly timescale in a region strongly impacted by BVOC using an iodide-adduct ionization HRToF-CIMS coupled to an FIGAERO inlet during the SOAS campaign. Highly functionalized pONs containing between six and eight oxygen atoms dominated the mole fraction in each carbon atom number group. The molecular speciation provides unique insights into the sources and evolution of pON and specifically, a strong connection to BVOC precursors. Diel profiles of the speciated pON were consistent with that of the presumed gaseous BVOC. We can simulate the

diel behavior of absolute and relative contributions of C_5 and C_{10} nitrates assuming gas-phase production of the highly functionalized pONs as early generation products of BVOC oxidation that rapidly establish gas–particle equilibrium together with a relatively fast pON loss rate corresponding to a lifetime of 2–4 h. Given the observed pON loadings during the SOAS, such a short lifetime of pON suggests a flux of organic carbon through aerosol particles each day that is on the order of observed OA mass concentrations and a cycling of NO_x that is on the order of the HNO_3 production rate from OH + NO_2. Thus, the chemical fates of pON need to be elucidated to accurately quantify the associated impacts.

ACKNOWLEDGMENTS. We thank all of the Southern Oxidant and Aerosol Study (SOAS) team members, in particular Annmarie G. Carlton (Rutgers University) and Steve B. Bertman (Western Michigan University). We thank Paul O. Wennberg (California Institute of Technology) for helpful suggestions on analysis. We also thank Matthieu Riva and Jason Surratt (University of North Carolina, Chapel Hill) for allowing us access to their sulfated ON dataset. The FIGAERO HRToF-CIMS was developed with funding from the US Department of Energy Small Business Innovation and Research Program Grant DE-SC0004577 (to J.A.T.) and Atmospheric System Research Program Grants DE-SC0006867 (to J.A.T.) and DE-SC0011791 (to J.A.T.). Its deployment at the SOAS campaign was supported by National Science Foundation (NSF) CAREER Award ATM-0846183 (to J.A.T.). The University of Gothenburg group was supported by Swedish Research Council Formas Grant 214-2010-1756. The University of Helsinki group was supported by the Academy of Finland. Funding for B.H.L. was provided by the National Oceanic and Atmospheric Administration Climate (NOAA) and Global Change Postdoctoral Fellowship Program. The University of California, Berkeley group was supported by NSF Grants AGS-1120076 (to R.C.C.) and AGS-1352972 (to R.C.C.). The Georgia Institute of Technology group was supported by NSF Grant 1242258 (to R. J. Weber) and US Environmental Protection Agency (EPA) STAR Grants RD-83540301 (early career; to N.L.N.) and R835410 (to N.L.N.). The University of Colorado Boulder group was supported by NSF Grant AGS 1243354 (to J.L.J.) and NOAA Grant NA13OAR4310063 (to J.L.J.). The University of California, Irvine group was supported by US EPA STAR Research Program R835400 (S.K.). The Pacific Northwest National Laboratory group was supported by the US Department of Energy Atmospheric System Research Program (J.E.S.). The Purdue University group was supported by NSF Grant AGS 1228496 (to P.B.S.). The University of California, Berkeley group was supported by NSF Grant AGS-1250569 (to A.H.G.) and EPA STAR Grant 835407 (to A.H.G.). Funding for the SOAS ground site was provided by Southern Company and the Electric Power Research Institute.

1. Horowitz LW, Liang J, Gardner GM, Jacob DJ (1998) Export of reactive nitrogen from North America during summertime: Sensitivity to hydrocarbon chemistry. *J Geophys Res* 103(D11):13451–13476.
2. Liang J, et al. (1998) Seasonal budgets of reactive nitrogen species and ozone over the United States, and export fluxes to the global atmosphere. *J Geophys Res* 103(D11): 13435–13450.
3. Beaver MR, et al. (2012) Importance of biogenic precursors to the budget of organic nitrates: Observations of multifunctional organic nitrates by CIMS and TD-LIF during BEARPEX 2009. *Atmos Chem Phys* 12(13):5773–5785.
4. Browne EC, et al. (2013) Observations of total $RONO_2$ over the boreal forest: NO_x sinks and HNO_3 sources. *Atmos Chem Phys* 13(9):4543–4562.
5. Paulot F, Henze DK, Wennberg PO (2012) Impact of the isoprene photochemical cascade on tropical ozone. *Atmos Chem Phys* 12(3):1307–1325.
6. Perring AE, Pusede SE, Cohen RC (2013) An observational perspective on the atmospheric impacts of alkyl and multifunctional nitrates on ozone and secondary organic aerosol. *Chem Rev* 113(8):5848–5870.
7. Farmer DK, et al. (2010) Response of an aerosol mass spectrometer to organonitrates and organosulfates and implications for atmospheric chemistry. *Proc Natl Acad Sci USA* 107(15):6670–6675.
8. Ng NL, et al. (2007) Effect of NO_x level on secondary organic aerosol (SOA) formation from the photooxidation of terpenes. *Atmos Chem Phys* 7(19):5159–5174.
9. Nguyen TB, Laskin J, Laskin A, Nizkorodov SA (2011) Nitrogen-containing organic compounds and oligomers in secondary organic aerosol formed by photooxidation of isoprene. *Environ Sci Technol* 45(16):6908–6918.
10. Perraud V, et al. (2012) Nonequilibrium atmospheric secondary organic aerosol formation and growth. *Proc Natl Acad Sci USA* 109(8):2836–2841.
11. Rollins AW, et al. (2012) Evidence for NO_x control over nighttime SOA formation. *Science* 337(6099):1210–1212.
12. Ehn M, et al. (2014) A large source of low-volatility secondary organic aerosol. *Nature* 506(7489):476–479.
13. Capouet M, Müller J-F (2006) A group contribution method for estimating the vapour pressures of α-pinene oxidation products. *Atmos Chem Phys* 6:1455–1467.
14. Lee BH, et al. (2014) An iodide-adduct high-resolution time-of-flight chemical-ionization mass spectrometer: Application to atmospheric inorganic and organic compounds. *Environ Sci Technol* 48(11):6309–6317.
15. Lopez-Hilfiker FD, et al. (2014) A novel method for online analysis of gas and particle composition: Description and evaluation of a Filter Inlet for Gases and AEROsols (FIGAERO). *Atmos Meas Tech* 7(4):983–1001.
16. Attwood AR, et al. (2014) Trends in sulfate and organic aerosol mass in the Southeast U.S.: Impact on aerosol optical depth and radiative forcing. *Geophys Res Lett* 41(21):7701–7709.
17. Washenfelder RA, et al. (2015) Biomass burning dominates brown carbon absorption in the rural southeastern United States. *Geophys Res Lett* 42(2):653–664.
18. Xu L, et al. (2015) Effects of anthropogenic emissions on aerosol formation from isoprene and monoterpenes in the southeastern United States. *Proc Natl Acad Sci USA* 112(1):37–42.
19. Lopez-Hilfiker FD, et al. (2015) Phase partitioning and volatility of secondary organic aerosol components formed from α-pinene ozonolysis and OH oxidation: The importance of accretion products and other low volatility compounds. *Atmos Chem Phys* 15(14):7765–7776.
20. Lee L, Teng AP, Wennberg PO, Crounse JD, Cohen RC (2014) On rates and mechanisms of OH and O_3 reactions with isoprene-derived hydroxy nitrates. *J Phys Chem A* 118(9):1622–1637.
21. Francisco MA, Krylowski J (2005) Chemistry of organic nitrates: Thermal chemistry of linear and branched organic nitrates. *Ind Eng Chem Res* 44(15):5439–5446.
22. Day DA, Wooldridge PJ, Dillon MB, Thornton JA, Cohen RC (2002) A thermal dissociation laser-induced fluorescence instrument for in situ detection of NO_2, peroxy nitrates, alkyl nitrates, and HNO_3. *J Geophys Res*, 10.1029/2001JD000779.
23. Rollins AW, Smith JD, Wilson KR, Cohen RC (2010) Real time in situ detection of organic nitrates in atmospheric aerosols. *Environ Sci Technol* 44(14):5540–5545.
24. Fry JL, et al. (2013) Observations of gas- and aerosol-phase organic nitrates at BEACHON-RoMBAS 2011. *Atmos Chem Phys* 13(17):8585–8605.
25. Orsini DA, et al. (2003) Refinements to the particle-into-liquid sampler (PILS) for ground and airborne measurements of water soluble aerosol composition. *Atmos Environ* 37(9-10):1243–1259.
26. Surratt JD, et al. (2008) Organosulfate formation in biogenic secondary organic aerosol. *J Phys Chem A* 112(36):8345–8378.
27. Xu L, Suresh S, Guo H, Weber RJ, Ng NL (2015) Aerosol characterization over the southeastern United States using high-resolution aerosol mass spectrometry: Spatial and seasonal variation of aerosol composition and sources with a focus on organic nitrates. *Atmos Chem Phys* 15(13):7307–7336.
28. Epstein SA, Blair SL, Nizkorodov SA (2014) Direct photolysis of α-pinene ozonolysis secondary organic aerosol: Effect on particle mass and peroxide content. *Environ Sci Technol* 48(19):11251–11258.
29. Müller J-F, Peeters J, Stavrakou T (2014) Fast photolysis of carbonyl nitrates from isoprene. *Atmos Chem Phys* 14(5):2497–2508.
30. Boyd CM, et al. (2015) Secondary organic aerosol formation from the β-pinene+NO_3 system: Effect of humidity and peroxy radical fate. *Atmos Chem Phys* 15(13):7497–7522.
31. Cole-Filipiak NC, O'Connor AE, Elrod MJ (2010) Kinetics of the hydrolysis of atmospherically relevant isoprene-derived hydroxy epoxides. *Environ Sci Technol* 44(17):6718–6723.
32. Darer AI, Cole-Filipiak NC, O'Connor AE, Elrod MJ (2011) Formation and stability of atmospherically relevant isoprene-derived organosulfates and organonitrates. *Environ Sci Technol* 45(5):1895–1902.
33. Rindelaub JD, McAvey KM, Shepson PB (2015) The photochemical production of organic nitrates from α-pinene and loss via acid-dependent particle phase hydrolysis. *Atmos Environ* 100:193–201.
34. George IJ, Abbatt JPD (2010) Heterogeneous oxidation of atmospheric aerosol particles by gas-phase radicals. *Nat Chem* 2(9):713–722.
35. Lee AKY, Herckes P, Leaitch WR, Macdonald AM, Abbatt JPD (2011) Aqueous OH oxidation of ambient organic aerosol and cloud water organics: Formation of highly oxidized products. *Geophys Res Lett* 38:L11805.
36. Ehn M, et al. (2012) Gas phase formation of extremely oxidized pinene reaction products in chamber and ambient air. *Atmos Chem Phys* 12(11):5113–5127.
37. Nah T, Sanchez J, Boyd CM, Ng NL (2015) Photochemical aging of α-pinene and β-pinene secondary organic aerosol formed from nitrate radical oxidation. *Environ Sci Technol*, 10.1021/acs.est.5b04594.
38. Horii CV, et al. (2004) Fluxes of nitrogen oxides over a temperate deciduous forest. *J Geophys Res* 109:D08305.
39. Min KE, et al. (2014) Eddy covariance fluxes and vertical concentration gradient measurements of NO and NO_2 over a ponderosa pine ecosystem: Observational evidence for within-canopy chemical removal of NO_x. *Atmos Chem Phys* 14(11):5495–5512.
40. Atkinson R, Aschmann SM, Carter WPL, Winer AM, Pitts JN (1982) Alkyl nitrate formation from the NO_x-air photooxidations of C_2-C_8 N-alkanes. *J Phys Chem* 86(23):4563–4569.
41. Darnall KR, Carter WPL, Winer AM, Lloyd AC, Pitts JN (1976) Importance of RO_2+NO in alkyl nitrate formation from C_4-C_6 alkane photooxidations under simulated atmospheric conditions. *J Phys Chem* 80(17):1948–1950.
42. Fry JL, et al. (2014) Secondary organic aerosol formation and organic nitrate yield from NO_3 oxidation of biogenic hydrocarbons. *Environ Sci Technol* 48(20):11944–11953.
43. Gallagher MW, et al. (1997) Measurements of aerosol fluxes to Speulder forest using a micrometeorological technique. *Atmos Environ* 31(3):359–373.
44. Jacobs MI, Burke WJ, Elrod MJ (2014) Kinetics of the reactions of isoprene-derived hydroxynitrates: Gas phase epoxide formation and solution phase hydrolysis. *Atmos Chem Phys* 14(17):8933–8946.
45. Liu S, et al. (2012) Hydrolysis of organonitrate functional groups in aerosol particles. *Aerosol Sci Technol* 46(12):1359–1369.
46. Reisinger AR (2000) Observations of HNO_2 in the polluted winter atmosphere: Possible heterogeneous production on aerosols. *Atmos Environ* 34(23):3865–3874.
47. Hu KS, Darer AI, Elrod MJ (2011) Thermodynamics and kinetics of the hydrolysis of atmospherically relevant organonitrates and organosulfates. *Atmos Chem Phys* 11(16):8307–8320.